DOI:
10.1093/schbul/sbw110

Document Version
Peer reviewed version

Structural network disorganization in subjects at clinical high risk for psychosis

André Schmidt,[1] Nicolas A. Crossley,[1] Fabienne Harrisberger,[2] Renata Smieskova,[2] Claudia Lenz,[2] Anita Riecher-Rössler,[2] Undine Lang,[2] Philip McGuire,[1] Paolo Fusar-Poli,[1] Stefan Borgwardt[1,2]

[1] Department of Psychosis Studies, King's College London, Institute of Psychiatry, Psychology and Neuroscience, London, UK

[2] Department of Psychiatry (UPK), University of Basel

Corresponding author: André Schmidt, Ph.D., Department of Psychosis Studies, Institute of Psychiatry, Psychology and Neuroscience, PO63 De Crespigny Park, London SE5 8AF, phone: +44 (0) 77 8666 6570, fax: +44 (0) 20 7848 0976, e-mail: andre.schmidt@kcl.ac.uk

Running title: Rich-club connectivity in the psychosis high-risk state

Word count abstract: 218

Word count text (including abstract): 3992

Abstract

Previous network studies in chronic schizophrenia patients revealed impaired structural organization of the brain's rich-club members, a set of highly interconnected hub regions that play an important integrative role for global brain communication. Moreover, impaired rich-club connectivity has also been found in unaffected siblings of schizophrenia patients, suggesting that abnormal rich-club connectivity is related to familiar, possibly reflecting genetic, vulnerability for schizophrenia. However, no study has yet investigated whether structural rich-club organization is also impaired in individuals with a clinical risk syndrome for psychosis. Diffusion tensor imaging and probabilistic tractography was used to construct structural whole-brain networks in 24 healthy controls and 24 subjects with an at-risk mental state (ARMS). Graph theory was applied to quantify the structural rich-club organization and global network properties. ARMS subjects revealed a significantly altered structural rich-club organization compared with the control group. The disruption of rich-club organization was associated with the severity of negative psychotic symptoms and led to an elevated level of modularity in ARMS subjects. This study shows that abnormal structural rich-club organization is already evident in clinical high-risk subjects for psychosis and further demonstrates the impact of rich-club disorganization on global network communication. Together with previous evidence in chronic schizophrenia patients and unaffected siblings, our findings suggest that abnormal structural rich-club organization may reflect an endophenotypic marker of psychosis.

Key words: psychosis, clinical high-risk, structural connectivity, network, rich-club, graph theory

Introduction

Recent network studies propose that connectivity abnormalities in schizophrenia are not solely attributable to changes in local regions and connections, but rather emerge from an aberrant topology of the network as a whole, the connectome of the brain.[1-3] Such graph theoretic mapping techniques have emerged as a very helpful approach to infer complex network properties of the healthy brain [4] and to understand the pathoconnectomic of psychiatric disorders.[5-7] For instance, consistent with reports in chronic schizophrenia patients,[8-13] recent network studies derived from whole-brain graph analyses showed reduced levels of structural global efficiency, reflecting the capacity for network-wide information processing,[4] in non-help seeking individuals with psychotic experiences[14] and in different populations at increased genetic risk for schizophrenia.[15-18]

One major contribution of graph theory to our understanding of neuropsychiatric diseases has been in highlighting the important role of hubs, which are nodes of the network with an unusually high number or strength of connections.[19] It has been shown that some of these brain hubs tend to be more densely interconnected among themselves than would be expected solely from their high degree, forming together a 'rich-club'.[20] These members of the brain's rich-club serve as a macroscopic anatomical substrate to cross-link functional networks and thus play an important role in the integration of information between segregated functional domains of the human cortex.[21] The high level of centrality of brain hubs also renders them points of vulnerability that are susceptible to disconnection and dysfunction in psychosis.[6, 7, 22] Using diffusion tensor imaging (DTI) and resting state fMRI data, reduced interconnectedness of rich-club regions has been detected in established schizophrenia, which was found to be associated with lower levels of global communication capacity.[9] This study provided novel biological evidence that schizophrenia is characterized by a selective disruption of structural brain connectivity among central brain hubs, potentially leading to reduced communication capacity and altered functional brain dynamics.[9] Moreover, abnormal rich-club organization is already evident in unaffected siblings of schizophrenia patients if compared with healthy subjects, but less affected than in schizophrenia patients.[23] This study suggested that

impaired rich-club connectivity is related to familial, possibly reflecting genetic, vulnerability for schizophrenia.[23]

The present DTI study examined whether structural rich-club organization is also affected in 24 subjects with a clinical high-risk syndrome for psychosis (see[24] for a comprehensive review of the international criteria), in particular with an at-risk mental state (ARMS), compared to 24 healthy controls. While first-degree relatives of schizophrenia patients have approximately a 10-fold increased risk for developing psychosis over lieftime,[25, 26] subjects at clinical high-risk have a high probability of transitioning to overt psychosis (mostly schizophrenia spectrum disorders[27]) within a short period (36% within 3 years of presentation).[28] We also assessed global network properties including efficiency and modularity to explore whether they were related to rich-club connectivity across all participants. Although previous research showed that lower levels of structural rich-club connectivity were related to worse overall functioning in chronic schizophrenia patients,[23] no study has yet investigated the impact of abnormal rich-club organization on global functioning and subclinical psychotic symptoms in ARMS subjects. To address this point, we finally tested the relationship of structural rich-club organization to positive and negative attenuated psychotic symptoms, as well as to deficits in global functioning in ARMS subjects. Our first hypothesis was that ARMS subjects would reveal aberrant rich-club organization compared with healthy controls and that this disruption would be associated with abnormal global network properties. Secondly, we hypothesized a negative relationship between the level of rich-club organization and the severity of attenuated psychotic symptoms and impairments in global functioning in ARMS subjects.

Methods and Materials

Participants

We recruited 24 healthy controls (HCs) and 28 ARMS subjects in our specialised clinic for the early detection of psychosis at the Department of Psychiatry, University of Basel (UPK), Switzerland. All participants provided written informed consent, and the study had research ethics committee permission. We assessed subjects using the 'Basel Screening Instrument for Psychosis' (BSIP),[29] the Brief Psychiatric Rating Scale (BPRS),[30] the Scale for the Assessment of Negative Symptoms (SANS)[31] and the Global Assessment of Functioning (GAF). We additionally obtained current and previous psychotropic medication, as well as nicotine and illegal drug consumption, by using a semi-structured interview (www.eppic.org.au). These exclusion criteria were applied to all groups: history of previous psychotic disorder; psychotic symptomatology secondary to an organic disorder; substance abuse according to ICD-10 research criteria; psychotic symptomatology associated with an bipolar disorder or major depression or a borderline personality disorder; age under 18 years; inadequate knowledge of the German language; and IQ less than 70.[32]

According to the Personal Assessment and Crisis Evaluation (PACE)[33] and the international standard criteria,[24] inclusion for an ARMS required one or more of the following: a) attenuated psychotic-like symptoms, b) brief limited intermittent psychotic symptoms (BLIPS) or c) a first or second degree relative with a psychotic disorder plus at least two further risk factors for or indicators of beginning psychosis according to the BSIP screening instrument, such as deterioration in social functioning. Inclusion because of attenuated psychotic symptoms required that change in mental state had to be present at least several times a week and for more than 1 week (a score of 2 or 3 on the BPRS hallucination item, or 3 or 4 on BPRS items for unusual thought content or suspiciousness). Inclusion because of BLIPS required scores of 4 or above on the hallucination item, or 5 or above on the unusual thought content, suspiciousness or conceptual disorganisation items of the BPRS, with each symptom lasting less than one week before resolving spontaneously. After the baseline assessment, the ARMS subjects were followed up clinically and received standard psychiatric case management.

Five ARMS individuals have transited to psychosis. All ARMS individuals were antipsychotic-naïve and 11 received low dose antidepressants.

DTI data acquisition and preprocessing

Details on DTI data acquisition and preprocessing can be found in the supplement.

Weighted connectome reconstruction

See Supplementary Figure 1 for an overview of the analytical workflow.

Network node definition: Freesurfer software[34] was applied to the individual T1 images to parcellate the brain surface into 68 cortical and 14 subcortical regions (41 per hemisphere), as previously done.[9, 20] The 82 segmented regions (see Supplementary Table 1) for each participant were then coregistered to the individual DTI reference image with b=0s/mm2.

Tractography-based structural connections: We used the output of a probabilistic tractography algorithm to define the weights of the connections, building a weighted network. Probabilistic tractography methods probe the fiber orientation probability distributions at each voxel, assessing the likelihood of a fiber following a particular path given the diffusion data. Advantages of this method over the deterministic method include the ability to explicitly represent uncertainty in the data[35] and that it can more reliably reconstruct crossing fibers.[36] Probabilistic tractography was carried out using bedpostX/probtrackX.[35] BedpostX uses Monte Carlo Markov chain sampling to estimate the diffusion parameters at each voxel and also calculates the necessary parameters for probabilistic tractography. The probabilistic tractography (probtrackX) was applied by sampling 5000 streamline fibers per voxel, thus for each region (node hereafter), 5000 x n fibers were sampled where n is the number of voxels in the node. Results from the probabilistic tractography algorithm are dependent on the seeding position. This implies that the connectivity index calculated from node i to j is not the same as the one from j to i. However, these are highly correlated across the brain regions for all subjects (median R=0.86, 95% confidence interval=[0.71; 0.94]). We therefore followed previous authors[37, 38] and defined the unidirectional connectivity probability P_{ij} between node i and j by averaging these two probabilities. However, the size of a node may influence the fiber selection

procedure: bigger seed regions would have more voxels where streamlines would be started, and bigger target regions may have a higher probability of being touched by one of the fiber streamlines. To control for this effect, the number of streamlines between node i and j was normalized by the product of the voxel number of node i and j.

Weighted rich-club effect

The rich-club phenomenon in networks alludes to the tendency of the highly connected nodes to establish more or stronger links among themselves than randomly expected.[39, 40] In brief, the weighted rich-club coefficient $\Phi^w(r)$ is computed as the sum of the weights of the subset of connections $E_{>r}$ of the nodes with a richness factor > r in the network divided by the sum of the set of the strongest $E_{>r}$ connections in the total network.[40] Furthermore, to assess the actual presence of the weighted rich-club phenomenon, discounted of random expectations, $\Phi^w(r)$ must be compared to the averaged rich-club curve $\Phi^w_{random}(r)$ of a (set of) comparable random network(s) to determine the extent to which empirically observed connection density between rich-club nodes exceeds that predicted by a random null model.[39, 40] In this study $\Phi^w_{random}(r)$ was computed for each level of r by averaging the rich-club coefficient over 1000 random network, in which the degree and strength distributions were preserved.[41] As such, this normalized rich-club value describes how much the network organization departs from the null model, controlling for the level of connectivity, which might be subject-specific. A normalized coefficient $\Phi^w_{norm}(r)$ (given as the ratio $\Phi^w(r)/\Phi^w_{random}(r)$) of > 1 over a range of r suggests the existence of rich club organization in a network.[40]

In this study r was defined as the node strength (computed as the sum of the weights of the node's connections). We were interested in looking at configurational aspects of the brain network, or the way connections are organized in the network. That meant we were not looking at differences introduced by the absolute level of connectivity across subjects. To further control for a global difference in the level of connectivity between groups (i.e., one group having stronger connections across the whole brain), we therefore computed Φ^w_{norm} as a function of percentiles of the node strength for each subject, ranging from 5-95% (rich-club level r). In other words, we computed Φ^w_{norm}

for each subject looking at the tendency of the network to concentrate its strongest connections in the *X* percentile of most connected regions. This ensured that irrespective if one subject had an overall much greater connectivity than another one, we would still be comparing whether their top *X* hubs were concentrating the stronger connections.

Statistical analysis of rich-club organization

First, two-tailed Wilcoxon rank-sum tests in Matlab (mathworks.com) were used to verify the existence of rich-club organization in each group, where $\Phi^{w}_{norm}(r)$ was significantly larger than zero (p value corrected for the number of rich-club levels, i.e. 19). Group differences in $\Phi^{w}_{norm}(r)$ were explored using permutation testing (10000) (p value corrected for the number of rich-club levels). To further test for group differences across different rich-club levels, permutation testing was also performed on the area under the rich-club curve (above 1).

Second, rich-club regions were then defined by selecting for each control subject the top 15% nodes, given their node strengths. This decision was based on the permutation test revealing that the group difference in $\Phi^{w}_{norm}(r)$ was most pronounced at the 85% level. This is in line with previous studies defining the top 12% as rich-club regions, given their node degree.[9, 20] Only those nodes evident in 85% of HCs were finally selected as rich-club regions. Accordingly, edges were classified into 'rich-club connections', being those edges that link members of the rich-club; 'feeder connections', which are the edges that link rich-club nodes to peripheral nodes; and 'local connections', being those edges that interconnect peripheral nodes. Permutation testing was then used to test for group differences between HCs and the ARMS sample.

Modularity, efficiency and clustering

We also examined the characterization of community (module) structure in the network, meaning the appearance of densely connected groups of nodes, with only sparser connections between groups [42] and global efficiency. Furthermore, we explored local efficiency and clustering (the level of local connectedness of a node) of the rich-club regions. All metrics were computed using the Brain

Connectivity Toolbox[41] based on the individually weighted networks and normalized with the same metrics of a set of random networks (n = 1000). Group differences in these graph metrics between HCs and ARMS subjects as a whole group were examined using permutation tests (10000).
Exploratory Pearson correlations were performed to explore the relationships between participants' rich-club organization (across rich-club levels, as indexed by the area under the curve) and global and local network metrics.

Relationship between rich-club organization and clinical features

In ARMS subjects, we tested for potential relationships between the level of rich-club organization and positive (sum of BPRS items 9 (suspiciousness), 10 (hallucinations), 11 (unusual thought content) and 15 (conceptual disorganization)) and negative (SANS total score) symptoms, as well as global functioning (GAF scores) using Pearson correlations. Findings from the correlational analyses in ARMS subjects are corrected for the total number of performed tests ($p<0.05/3$).
Across all participants, we further tested for relationships between rich-club organization, global network metrics, and global functioning using Pearson correlations. Correlation analyses across all participants are also corrected for the number of performed tests ($p<0.05/3$).

Results

Demographical and clinical features

The two groups did not differ in age, handedness, education, premorbid IQ and cigarette, alcohol or cannabis consumption, but they differed in gender (Table 1). As groups differed in gender, this variable was added as a covariate for all group comparisons of network measures.

Insert Table 1 about here

Rich-club organization

A rich-club organization in the structural network was detected in both groups, i.e. normalized rich-club coefficient (Φ^{w}_{norm}) > 1 over a range of r; the rich-club regime ranged from r=40 to r=95 in HCs (p's<0.0001) and from r=55 to r=90 in ARMS subjects (p's<0.0014) (Figure 1). Compared with HCs, ARMS subjects revealed a significantly reduced Φ^{w}_{norm} at level 85 (p=0.0251, corrected for the number of rich-club levels). The area under the rich-club curve was also significantly reduced in ARMS subjects compared with HCs (p=0.0120), reflecting a lower tendency for the strongest connections to be shared among the hubs of the brain in these subjects.

Insert Figure 1 about here

The rich-club comprised 8 regions, including the bilateral putamen, pallidum, accumbens and the left caudate and amygdala (Figure 2A). We found that ARMS subjects showed significantly reduced mean strength of rich-club connections (p=0.0207, corrected for the number of connections) compared with HCs (Figure 2B), whereas no group difference in the strength of feeder connections was found (p=0.9382) (Figure 2C). Of note, no volumetric group differences were found in rich-club regions (Supplementary Table 2). Furthermore, there was a statistical trend for increased strength of local connections in ARMS subjects (p=0.0549) compared with HCs (Figure 2D).

Insert Figure 2 about here

Modularity, efficiency and clustering

Structural networks of ARMS subjects revealed an elevated level of modularity compared with HCs (p=0.0272) (Figure 3A). Correcting for the area under the rich-club curve this group effect was no longer evident (p=0.1313). Across all participants, we found a negative correlation between the area under the rich-club curve and modularity (r=-0.385, p=0.007) (Figure 3B). Groups did not differ in global efficiency (p=0.2613).

Furthermore, corrected for the number of rich-club regions, we found significantly reduced local efficiency of the right accumbens (p=0.0062) (Figure 3C) and a statistical trend for reduced local efficiency of the left putamen (p=0.090) in ARMS subjects compared with HCs. There was also a strong statistical trend for reduced clustering of the left amygdala (p=0.0532) and significantly reduced clustering of the left accumbens (p=0.0059) (Figure 3D). Finally, across all participants, there were significant positive correlations between rich-club organization and local efficiency of the right accumbens (r=0.328, p=0.023) and local clustering of the left accumbens (r=0.473, p=0.001) and left amygdala (r=0.449, p=0.001).

Insert Figure 3 about here

Relation between rich-club organization, global functioning and symptomatology

In ARMS subjects, there was a significant negative correlation between the area under the rich-club curve and negative psychotic symptoms (SANS total score; r=-0.506, p=0.012, corrected for multiple correlations) (Figure 4A) but not positive psychotic symptoms (r=0.023, p=0.914) and global functioning (GAF score; r=0.222, p=0.298).

Across all participants, global functioning correlated positively with the area under the rich-club curve (r=0.440, p=0.002, corrected for multiple correlations) (Figure 4B) and negatively with modularity (r=-0.305, p=0.035, uncorrected for multiple correlations) (Figure 4C).

Insert Figure 4 about here

Discussion

To our knowledge, this is the first graph theoretical DTI study in clinical high-risk subjects for psychosis. The main finding of this study is impaired structural rich-club organization in clinical high-risk subjects for psychosis compared with healthy controls. This result extends previous findings in schizophrenia patients[9] and unaffected siblings[23] and also resonates with a study in individuals with a chromosome 22q11.2 deletion syndrome reporting reduced connectivity strength among A-core regions, which exhibited stronger-than-expected interconnectivity and thus resemble a weighted rich-club.[16] These findings together support the notion that a breakdown of hub network connectivity may constitute a core pathoconnectomical hallmark of psychosis[6, 7, 22] and already exists in clinical high-risk samples, suggesting the potential of network connectivity measures to predict outcomes in psychosis.[43-46]

The second major finding was that the level of rich-club disorganization in ARMS subjects correlated with the severity of negative symptoms, which may also have some translational impact, given that negative symptoms are refractory to all available treatments.[47] The identified rich-club regions in this study comprised the dorsal and ventral striatum, the globus pallidus and the amygdala. Consistent with a previous meta-analysis[48] and multicentre study in subjects at clinical high-risk for psychosis,[49] we found no volumetric group differences in these regions, indicating that the group difference in rich-club organization was not due to microstructural changes in these regions. Across the rich-club regions, we found that ARMS subjects revealed significantly reduced local efficiency of the right accumbens and a trend for reduced efficiency of the left putamen, while they also showed significantly reduced clustering of the left accumbens and a strong statistical trend for reduced clustering of the left amygdala. Notably, rich-club organization was positively related to local efficiency of the right accumbens and local clustering of the left accumbens and left amygdala across all participants, suggesting that the reduced strength of rich-club connections in ARMS subjects is probably associated with reduced local efficiency and clustering of the bilateral accumbens and the left amygdala. It has long been proposed that altered dopaminergic projections within the limbic-

striatal circuitry affect emotional and motivational behaviour in schizophrenia.[50, 51] Striatal dopamine function is abnormally elevated in both schizophrenia and in high-risk subjects[52-54] and the aberrant salience hypothesis proposes that this causes attribution of salience to contextually irrelevant stimuli but also to reduced attribution of salience to relevant cue features such as reward-indicating cues.[55, 56] A recent meta-analysis showed that reduced ventral striatal activation in response to reward-predicting cues correlated with the severity of negative symptoms in schizophrenia spectrum disorders.[57] Our finding of reduced structural limbic-striatal connectivity may thus reflect a scaffold for impaired reward-related salience processing in psychosis, which might contribute to the formation of negative symptoms. However, a lack of a significant relationship between abnormal structural rich-club connectivity and positive psychotic symptoms doesn't necessarily mean that no such relation exists. More studies with more accurate assessments of positive symptoms (e.g. SAPS) are needed to draw robust inferences on the relationship between abnormal structural rich-club organization and the formation of psychotic symptoms.

The limbic-striatal regions identified as rich-club members in the present study overlap with rich-club regions from recent DTI studies,[16, 58] but they also differ from other established rich-club regions, which included the bilateral thalamus, precuneus, superior frontal and superior parietal cortex, insula and hippocampus.[9, 20, 59] Different reasons may explain this discrepancy across studies and among others we like to mention a few potential explanations: First, network models have previously shown that rich-club members and their connections may substantially change with respect to the richness factor [40]. Second, different normalization strategies have been performed to adjust the streamline numbers for the size of the nodes/regions. While other studies normalized the streamlines connecting two regions of interest by the sum of their volumes,[9, 20, 59] the cortical surface area[16] or streamline length,[58] we normalized the streamline number by the product of the voxel numbers of node i and j. Third, there is no clear identified measure of what is a good index of structural strength.[60] In our study, the weight is based on the reliability with which the tracts were

reconstructed, which is different from the number of streamlines reconstructed (volume) used in previous studies.[9, 20]

Consistent with a finding in chronic patients,[9] we found an elevated level of modularity in high-risk subjects compared with healthy controls, reflecting a more segregated pattern of network organization. Notably, the increase in modularity was mediated by the disruption of rich-club organization in high-risk subjects, supporting the pivotal role of the rich-club in the integration of information between segregated brain modules.[21] Furthermore, albeit only at a statistical trend level, the strength of local connections was increased in ARMS subjects relative to healthy controls. These findings suggest that neural dysmodularity in clinical high-risk subjects is caused by a reduction in rich-club connectivity, which in turn may drive hyperconnectivity in peripheral regions.

Several issues merit comments. We used a probabilistic tractography method to map whole-brain white matter connectivity, which has advantages in tracking specific white matter tracts relating to fiber crossing compared with deterministic tractography methods.[36] However, such a probability-based approach could introduce spurious white matter connections that are biologically not connected. Consistent with other structural rich-club analyses,[9, 20, 23, 61] we decided not to threshold our individual connectivity matrices because a) every (or range of) statistical threshold is arbitrary and not informed by biological evidence, and b) small (and presumably false) edge weights will have inconsequential effects on the computed metrics.[8] However, new permutation-based methods may overcome the threshold issue in graph theoretical whole-brain analysis and are thus of interest for future network studies.[62] The small number of ARMS subject who developed psychosis limits the sensitivity of our exploratory analyses addressing psychosis transition. Ongoing multi-site projects in high-risk subjects may be best suited to test the generalizability of our findings. Finally, some of the ARMS subjects received low doses of antidepressants, which may have influenced our findings. In this study, the numbers of untreated and antidepressant-treated subjects were too small to allow for

meaningful sub-group analyses and this issue would be better addressed in longitudinal studies that were explicitly linked to study the effect of antidepressants on rich-club connectivity.

In summary, this study extends previous evidence in chronic patients [9] and unaffected siblings of schizophrenia patients[23] by showing impaired structural rich-club organization in clinical high-risk subjects for psychosis. It further highlights the role of structural rich-club connectivity as the backbone for network-wide information integration[21] and shows a breakdown of this interplay in clinical high-risk subjects for psychosis.

Supplementary Information

DTI data acquistion

Subjects were examined using a 3T magnetic resonance imaging scanner (Magnetom Verio, Siemens Healthcare, Erlangen, Germany). DTI data were acquired during 10 minutes, based on a single-shot echo planar imaging sequence with the following parameters: echo time/repetition time = 95/9200 ms, field of view = 320 mm and 54 axial slices of 2.5 mm slice thickness covering the whole brain with an in-plane resolution of 2.5 x 2.5 mm2. In addition, a 12-channel radio frequency head coil was used, as well as GRAPPA parallel imaging with an acceleration factor of 2, with phase partial Fourier of 6/8. In total, 30 isotropically distributed diffusion weighted directions with b-values of 900s/mm2 and one single reference image with b = 0s/mm2 were acquired twice as two averages. In addition, a high-resolution T1-weighted magnetization prepared rapid acquisition gradient echo (MPRAGE) image was acquired (TR = 2000 ms; TE = 3.37 ms; flip angle = 8°; inversion time = 1000 ms; 176 slices; slice thickness = 1 mm; voxel size = 1 x 1 x 1mm3).

DTI analysis was performed using FMRIB Diffusion Toolbox (FSL, version 5.0.7). In a first step, FSLView was used to visually check for potential artefacts in all directions. Directions displaying poor image quality (e.g. pulsation artefacts, venetian blind artefacts, inter-slice and intra-slice intensity artefacts, motion artefacts or extreme signal loss due to distortion issues) were subsequently excluded from further analysis. When subjects presented more than 10% bad directions, the complete data set was excluded (4 ARMS subjects). DTI data were then corrected for effects of motion and image distortions due to eddy currents by using an affine registration to the b = 0s/mm^2 volume. b-vectors were rotated according to the eddy current correction matrix. A brain mask was then created to remove non-brain tissue with the Brain Extraction Tool, and DTIFIT was used to reconstruct the diffusion tensor model at each voxel.

Supplementary Table 1. Brain regions and corresponding voxel numbers of the structural network in healthy controls and clinical high-risk subjects.

	Healthy controls (HC)																							
	HC01	HC02	HC03	HC04	HC05	HC06	HC07	HC08	HC09	HC10	HC11	HC12	HC13	HC14	HC15	HC16	HC17	HC18	HC19	HC20	HC21	HC22	HC23	HC24
Thalamus L	518	497	500	538	495	493	420	486	504	497	490	548	527	562	548	510	492	520	545	429	547	584	505	573
Caudate L	307	193	264	238	217	253	202	188	192	221	272	242	204	237	198	224	209	235	225	193	230	272	207	166
Putamen L	384	303	336	366	335	325	324	359	252	322	325	401	352	295	367	302	316	334	330	326	334	412	328	316
Pallidum L	103	89	100	100	95	88	81	97	73	102	93	118	95	81	112	73	86	99	114	94	88	121	98	103
Hippocampus L	275	259	252	314	249	259	229	275	255	243	259	304	257	262	242	281	315	268	254	238	261	281	274	282
Amygdala L	100	94	83	112	91	88	91	95	94	93	88	99	85	99	89	79	104	97	116	83	102	114	98	84
Accumbens L	34	25	23	30	28	28	23	27	16	24	27	42	27	29	32	28	28	22	31	32	36	37	21	21
Superior temporal L	166	140	147	208	179	152	128	135	136	128	99	225	153	241	160	163	128	142	142	97	217	191	145	152
Caudal anterior cingulate L	98	90	101	114	104	129	85	127	98	81	108	119	124	191	92	159	83	102	102	117	141	143	130	90
Caudal middle frontal L	472	404	453	393	363	327	360	375	360	362	367	444	415	543	474	336	301	355	327	361	484	555	524	286
Cuneus L	179	133	122	160	180	123	166	147	118	159	97	120	96	147	168	137	146	119	148	122	190	185	121	115
Entorhinal L	112	123	138	139	104	103	101	89	121	111	85	129	106	137	85	98	105	83	125	80	149	127	128	100
Fusiform gyrus L	674	666	546	692	662	628	535	629	491	611	523	619	486	704	584	604	597	508	573	601	706	848	545	460
Inferior parietal L	770	740	759	884	927	778	629	753	671	664	609	995	579	1213	843	778	782	646	818	684	800	928	854	720
Inferior temporal L	711	668	650	793	733	579	546	801	535	596	532	755	618	944	681	610	760	548	641	652	701	749	768	588
Isthums cingulate L	145	140	145	174	141	134	122	143	137	133	128	138	123	173	221	138	108	137	125	139	111	160	142	184
Lateral occipital L	786	645	742	688	748	758	616	846	568	610	546	714	446	795	839	616	740	594	598	590	841	834	786	744
Lateral orbitofrontal L	533	434	572	502	506	461	438	466	380	469	398	502	413	604	542	489	413	406	433	386	573	542	508	418
Lingual L	371	343	394	504	384	302	393	459	378	310	225	336	275	374	364	229	309	363	381	295	453	467	407	515
Medial orbitofrontal L	320	278	298	271	293	267	269	266	241	263	236	407	316	385	286	335	285	282	283	223	321	347	369	244
Middle temporal L	792	714	680	788	780	710	564	639	514	607	481	810	525	879	796	669	667	749	698	655	786	747	807	609
Parahippocampal L	117	129	97	149	132	145	148	136	112	103	121	147	99	169	131	138	158	133	105	98	128	142	168	150
Paracentral L	216	206	188	207	182	262	183	178	132	160	200	161	190	222	211	266	158	152	139	215	255	201	205	132
Parsopercularis L	323	210	307	261	325	279	280	300	259	248	302	299	279	328	343	345	284	265	245	344	270	280	333	272
Parsorbitalis L	152	115	132	151	127	140	154	137	112	135	112	142	103	145	190	122	142	112	128	140	165	167	129	135
Parstriangularis L	210	174	208	242	232	280	200	185	228	174	207	200	189	253	337	250	197	223	215	247	277	299	282	192
Pericalcarine L	136	88	120	116	95	86	110	106	91	118	69	88	48	89	102	87	105	75	103	106	129	124	82	75
Postcentral L	542	573	468	586	617	533	471	539	383	559	563	505	408	608	494	603	539	465	446	483	833	676	543	462
Posteriorcingulate L	221	215	155	199	196	180	172	220	136	135	168	227	185	244	156	208	183	142	189	186	256	221	176	181
Precentral L	805	841	741	851	745	782	739	810	641	724	766	827	743	918	714	829	744	673	666	770	969	885	873	688
Precuneus L	664	564	658	644	656	627	548	610	512	512	524	504	568	690	683	685	424	540	551	536	625	791	617	464
Rostral anterior cingulate L	144	136	198	172	162	157	139	137	136	147	154	169	164	270	212	180	204	158	176	157	163	218	163	153
Rostral middle frontal L	1083	976	1003	1084	994	924	887	933	755	1051	792	1062	951	1206	1321	1069	996	949	987	856	1250	1381	976	865
Superior frontal L	1602	1317	1306	1395	1451	1365	1292	1354	1058	1054	1225	1601	1184	1586	1490	1270	1333	1230	1182	1265	1527	1641	1695	1255
Superior parietal L	811	877	786	995	785	783	662	834	761	928	690	683	704	958	799	836	822	773	783	787	761	970	729	659
Superior temporal L	815	734	675	723	826	798	726	837	579	688	650	932	719	840	878	742	770	768	626	602	944	985	846	811
Supramarginal L	817	603	585	792	671	786	705	668	444	538	520	729	649	847	735	620	765	696	624	590	724	788	626	640
Frontal pole L	41	45	54	39	38	45	57	55	38	44	41	62	50	62	54	46	56	58	44	45	51	55	67	49
Temporal pole L	169	158	168	210	188	160	158	154	107	142	176	135	136	155	162	169	185	188	160	137	139	145	146	164
Transverse temporal L	83	54	65	71	74	95	54	65	44	78	72	70	49	68	78	73	50	62	62	56	74	64	79	76
Insula L	450	413	368	444	451	445	370	381	332	398	401	481	395	441	578	452	398	429	382	390	403	476	422	395
Thalamus R	463	459	476	514	453	469	424	455	473	474	488	546	463	491	525	456	451	479	548	434	553	557	467	524
Caudate R	299	193	244	218	200	249	181	180	166	205	240	225	186	254	216	196	201	211	220	186	209	286	181	161
Putamen R	353	315	323	326	338	290	293	334	254	305	308	344	340	301	332	288	291	338	337	296	334	397	332	337

Pallidum R	94	87	80	93	90	85	80	92	75	93	80	102	88	83	90	72	93	96	93	84	92	110	85	80
Hippocampus R	277	265	270	323	267	291	237	280	251	264	243	297	263	279	273	273	301	281	252	217	243	280	313	282
Amygdala R	104	101	82	101	95	73	79	85	88	82	90	109	95	98	79	83	100	90	116	86	110	108	95	95
Accumbens R	33	26	33	34	31	31	30	31	21	25	38	43	33	38	32	32	33	30	32	36	44	41	32	20
Superior temporal R	141	178	131	185	171	115	163	157	125	129	105	182	117	250	142	117	127	133	138	98	137	188	189	168
Caudal anterior cingulate R	170	92	84	56	134	106	136	119	80	107	123	143	69	192	86	129	142	62	107	115	205	214	120	121
Caudal middle frontal R	395	315	404	365	334	289	379	312	283	356	400	374	381	385	448	460	271	320	296	361	420	386	438	294
Cuneus R	192	146	164	129	158	167	154	124	130	163	127	132	108	186	156	162	75	172	135	147	167	207	161	58
Entorhinal R	84	131	130	136	117	96	74	118	82	79	89	117	89	194	97	98	117	86	127	116	122	105	83	54
Fusiform gyrus R	715	553	550	734	651	624	620	682	435	608	543	755	568	744	590	650	606	579	625	487	645	835	604	585
Inferiorparietal R	1098	1056	898	872	1085	925	773	907	738	856	886	1119	781	1167	1021	983	908	949	929	813	1065	1155	965	908
Inferiortemporal R	608	692	654	767	658	698	561	776	563	568	508	853	565	899	671	641	741	560	574	583	802	893	801	611
Isthums cingulate R	152	141	134	131	121	175	122	141	105	103	113	136	120	151	178	125	129	78	115	112	120	149	130	147
Lateraloccipital R	784	609	727	785	709	839	632	683	589	563	597	735	502	738	801	635	603	655	586	618	870	960	632	769
Lateralorbitofrontal R	539	528	475	509	465	466	403	410	342	431	439	472	444	560	524	460	443	416	456	390	518	502	460	402
Lingual R	370	378	389	502	419	328	317	417	378	363	302	356	257	417	347	232	346	381	351	307	453	449	369	450
Medialorbitofrontal R	343	302	333	365	337	248	260	268	234	287	263	329	291	366	367	362	356	291	319	258	353	395	371	269
Middletemporal R	931	661	778	854	950	720	742	738	604	680	532	853	665	1025	857	645	756	761	818	693	786	956	820	681
Parahippocampal R	124	124	113	178	127	111	109	158	105	102	125	159	95	182	126	145	131	124	130	102	147	168	131	136
Paracentral R	240	223	219	209	197	224	221	261	153	184	173	215	221	247	232	234	173	216	177	204	267	223	265	236
Parsopercularis R	309	160	214	260	228	210	229	291	171	198	255	340	226	262	288	230	187	209	311	257	274	287	284	196
Parsorbitalis R	164	168	162	170	167	194	135	153	143	171	145	135	162	220	189	175	197	154	204	151	204	206	152	144
Parstriangularis R	258	171	250	293	228	289	223	270	254	273	250	309	236	203	286	231	181	309	213	202	274	297	428	247
Pericalcarine R	149	91	159	122	109	87	138	112	116	143	93	107	39	129	118	103	62	85	103	98	147	135	87	66
Postcentral R	575	484	401	495	549	498	354	489	320	361	431	443	364	698	564	616	535	543	549	475	639	576	457	430
Posterior cingulate R	234	207	183	157	207	186	180	190	160	154	143	226	166	225	242	208	166	162	176	183	267	245	189	179
Precentral R	776	803	789	776	878	774	726	718	625	685	786	1034	744	1079	839	755	762	627	649	823	963	892	867	715
Precuneus R	682	588	629	716	668	619	555	593	525	567	557	633	555	746	712	655	658	406	587	541	660	797	643	457
Rostral anterior cingulate R	100	122	106	111	136	146	112	125	89	119	135	163	75	173	105	134	160	137	132	117	133	199	156	102
Rostral middle frontal R	1139	983	1023	958	880	831	796	849	842	963	866	895	906	1049	1102	1061	967	900	937	883	1300	1317	1091	976
Superior frontal R	1420	1260	1356	1536	1416	1346	1270	1359	982	1080	1128	1325	1254	1644	1553	1344	1370	1437	1207	1212	1412	1332	1556	1174
Superior parietal R	738	722	752	944	783	781	691	922	733	883	685	744	641	933	808	775	915	549	661	774	995	906	782	759
Superior temporal R	856	654	599	741	777	725	665	741	554	680	606	740	692	944	860	687	681	658	594	637	819	792	825	730
Supramarginal R	728	557	524	773	698	641	626	681	530	526	402	546	579	881	770	651	547	598	556	570	620	681	617	635
Frontal pole R	54	68	83	54	91	53	57	67	50	79	47	68	57	67	87	49	93	44	53	48	64	80	59	60
Temporalpole R	150	140	137	155	156	167	150	144	118	139	173	174	142	142	179	147	167	98	157	136	164	155	157	135
Transverse temporal R	43	50	51	66	60	69	55	57	32	53	42	64	37	50	52	58	44	57	30	37	59	44	44	67
Insula R	456	387	382	415	448	453	370	396	350	427	366	513	409	462	514	495	356	400	382	386	462	508	441	382
Thalamus R	518	497	500	538	495	493	420	486	504	497	490	548	527	562	548	510	492	520	545	429	547	584	505	573
Thalamus L	307	193	264	238	217	253	202	188	192	221	272	242	204	237	198	224	209	235	225	193	230	272	207	166

	Clinical high-risk (HR) subjects																							
	HR01	HR02	HR03	HR04	HR05	HR06	HR07	HR08	HR09	HR10	HR11	HR12	HR13	HR14	HR15	HR16	HR17	HR18	HR19	HR20	HR21	HR22	HR23	HR24
Thalamus L	415	521	585	496	461	534	527	496	487	513	526	562	531	560	539	494	482	565	445	626	563	460	465	504
Caudate L	189	261	250	183	229	228	254	229	231	279	277	218	238	246	273	249	244	257	203	284	241	231	235	312
Putamen L	307	384	286	289	400	403	339	362	356	339	398	305	342	360	350	369	339	334	258	418	321	332	311	362
Pallidum L	82	117	108	92	96	105	103	109	87	116	98	84	109	92	115	118	74	103	94	107	82	102	72	105
Hippocampus L	223	275	275	255	247	285	274	262	267	301	232	285	289	309	263	287	237	261	223	298	295	255	260	274
Amygdala L	86	102	81	92	93	104	115	106	90	99	99	114	96	110	100	91	93	69	62	107	98	109	92	100
Accumbens L	20	36	19	13	38	21	33	20	30	25	29	27	26	34	27	31	23	35	15	31	34	40	25	28

Superior temporal L	131	191	165	117	146	187	241	155	165	132	150	172	288	195	179	176	151	137	136	209	188	142	124	115
Caudal anterior cingulate L	107	129	95	134	114	82	156	138	160	155	89	107	121	166	65	113	65	153	134	145	117	113	98	102
Caudal middle frontal L	333	362	499	425	348	427	403	400	461	396	355	412	322	354	455	344	346	363	315	442	386	395	366	375
Cuneus L	102	117	158	137	121	161	192	133	172	218	111	139	163	202	165	155	92	155	124	177	160	140	144	149
Entorhinal L	88	142	135	119	117	101	119	111	121	122	105	153	92	98	92	103	116	116	111	112	132	116	95	110
Fusiform gyrus L	451	645	562	532	522	638	735	676	734	552	613	604	667	675	804	603	633	708	536	707	725	800	555	538
Inferior parietal L	556	780	980	785	808	696	951	728	959	844	743	870	971	772	883	806	807	941	722	946	863	804	838	630
Inferior temporal L	499	674	618	755	719	811	717	805	797	1000	671	739	776	689	702	772	684	760	701	730	910	779	644	638
Isthums cingulate L	119	157	182	140	118	166	177	153	161	161	103	126	134	161	140	182	104	135	148	250	176	128	117	150
Lateral occipital L	542	768	811	726	650	783	854	689	728	805	670	794	675	877	788	795	610	774	598	838	770	809	524	769
Lateral orbitofrontal L	418	492	542	357	487	551	523	459	565	588	426	538	470	557	521	446	441	520	408	516	577	508	451	484
Lingual L	277	316	360	392	327	397	457	428	383	481	351	405	386	295	452	432	236	335	321	365	498	314	316	407
Medial orbitofrontal L	217	316	274	219	256	347	317	270	396	314	224	326	307	320	325	289	225	339	217	358	376	303	249	257
Middle temporal L	493	811	624	667	766	632	839	725	819	1031	633	726	721	751	684	857	525	601	633	803	877	713	610	636
Parahippocampal L	102	112	115	106	114	127	129	147	98	118	121	113	132	156	145	127	154	110	93	118	126	148	122	140
Paracentral L	159	190	186	204	182	207	197	148	230	175	161	174	178	173	230	152	175	217	178	219	272	158	177	180
Parsopercularis L	238	316	329	383	273	438	382	246	471	328	221	337	300	284	323	397	276	368	207	333	324	282	232	358
Parsorbitalis L	137	122	127	117	127	157	145	156	159	220	122	173	141	183	130	162	130	128	116	157	188	170	114	148
Parstriangularis L	144	235	223	203	170	269	286	170	263	219	179	315	241	226	262	235	180	220	188	218	249	204	190	214
Pericalcarine L	67	83	94	119	101	92	133	106	106	125	78	121	100	111	118	129	54	104	59	138	142	75	105	74
Postcentral L	475	663	486	492	590	611	473	472	567	634	546	568	481	519	619	502	500	550	482	627	638	467	503	631
Posteriorcingulate L	146	234	176	200	180	222	215	209	160	233	193	217	214	162	246	189	173	233	179	195	216	157	151	154
Precentral L	588	797	856	530	858	846	936	734	843	929	791	848	782	873	848	705	691	760	608	888	810	702	790	920
Precuneus L	514	681	716	535	581	571	695	576	771	706	577	580	576	662	585	584	607	705	479	730	644	604	521	677
Rostral anterior cingulate L	148	184	176	181	175	186	198	165	233	210	153	193	164	196	147	157	151	188	161	262	254	159	147	156
Rostral middle frontal L	743	1029	1008	800	841	1150	1121	865	1096	1271	888	1101	1018	1189	1116	1162	871	1065	784	1341	1139	948	882	790
Superior frontal L	1259	1339	1338	1164	1384	1454	1535	1331	1587	1374	1351	1444	1441	1308	1390	1361	1341	1360	1068	1611	1518	1310	1269	1361
Superior parietal L	781	963	862	809	811	793	977	615	837	1066	763	890	750	962	756	921	801	819	751	976	1049	777	721	898
Superior temporal L	610	809	834	666	725	851	856	732	791	639	676	942	731	836	714	904	774	823	564	784	751	805	658	885
Supramarginal L	548	818	732	606	698	843	822	499	828	776	667	928	644	848	683	762	713	790	547	855	935	694	567	740
Frontal pole L	40	45	33	47	72	50	34	41	66	61	65	50	49	63	55	70	35	46	43	64	59	59	42	50
Temporal pole L	122	202	142	130	176	169	191	147	179	196	157	175	192	129	177	180	216	91	150	182	138	192	135	200
Transverse temporal L	55	63	62	43	56	98	63	51	61	41	58	69	61	84	67	70	81	103	57	56	66	71	50	79
Insula L	332	441	422	327	366	529	470	350	456	493	364	493	419	449	396	414	377	459	350	476	475	395	401	410
Thalamus R	387	499	556	425	458	508	483	481	491	506	494	540	499	519	555	489	465	544	403	602	544	455	439	558
Caudate R	191	276	257	171	218	203	247	227	205	275	236	221	227	237	243	244	211	232	190	245	246	204	242	278
Putamen R	292	367	294	285	402	359	344	339	343	347	377	306	336	351	338	366	297	342	286	437	314	305	321	333
Pallidum R	76	102	81	79	86	98	109	104	95	104	109	70	94	100	93	98	82	97	86	108	77	92	73	98
Hippocampus R	230	263	282	255	267	282	290	254	260	315	278	283	282	295	261	258	260	249	241	315	322	260	266	279
Amygdala R	73	93	91	82	92	101	104	95	97	110	99	89	94	107	86	89	89	84	77	100	118	109	80	94
Accumbens R	30	44	31	24	27	32	40	26	33	34	34	35	32	39	33	25	35	31	23	39	31	28	30	37
Superior temporal R	114	182	166	89	140	153	166	170	180	123	127	137	148	159	161	190	129	182	138	191	203	157	116	137
Caudal anterior cingulate R	87	165	107	104	93	155	127	115	226	112	76	116	140	146	165	75	84	126	70	148	164	118	140	92
Caudal middle frontal R	310	294	405	391	282	311	410	319	403	372	302	289	332	430	395	389	277	408	261	443	401	289	364	364
Cuneus R	148	185	191	161	144	164	218	137	153	247	90	149	180	195	203	78	108	175	163	192	188	169	144	171
Entorhinal R	85	147	107	110	63	61	132	92	109	122	117	124	127	134	88	86	131	109	75	106	125	137	115	113
Fusiform gyrus R	470	642	537	541	478	718	738	619	613	652	574	684	660	710	534	610	628	606	542	718	692	632	502	690
Inferiorparietal R	761	1027	896	906	1060	1003	1116	862	914	994	887	1088	1036	1039	1088	947	1027	1112	882	1138	1154	900	1001	1006
Inferiortemporal R	575	659	737	700	694	688	671	708	921	980	640	766	625	862	775	791	587	696	565	721	804	743	650	698
Isthums cingulate R	97	136	158	131	115	148	168	134	131	169	93	122	117	165	151	180	112	159	120	189	122	129	107	134
Lateraloccipital R	458	749	867	734	602	848	845	647	837	916	626	723	866	1000	747	725	688	787	621	781	756	785	563	712
Lateralorbitofrontal R	378	462	464	382	450	523	511	485	534	520	399	564	415	534	500	453	401	474	398	482	574	477	416	482
Lingual R	333	300	339	411	352	381	447	377	307	418	283	455	432	396	462	435	263	389	348	371	405	373	271	427
Medialorbitofrontal R	238	330	306	263	283	321	315	283	414	384	252	352	342	332	331	276	266	313	262	328	419	356	258	319
Middletemporal R	498	818	813	652	767	758	938	851	838	935	707	871	811	781	856	828	697	770	714	977	970	924	710	647

Parahippocampal R	96	115	115	122	116	89	155	138	106	141	137	135	141	134	115	114	108	119	103	115	133	165	105	139
Paracentral R	151	259	213	162	187	263	210	169	273	283	172	210	254	173	175	187	251	224	193	270	302	194	210	212
Parsopercularis R	216	270	220	234	277	240	234	186	305	278	240	252	211	282	294	219	218	253	232	206	250	235	271	283
Parsorbitalis R	137	152	183	141	150	188	158	190	158	197	117	177	179	189	172	143	172	197	142	200	218	204	117	156
Parstriangularis R	192	323	327	218	275	330	310	178	293	377	208	289	293	261	298	309	216	287	290	315	373	230	242	283
Pericalcarine R	95	112	143	104	112	92	132	109	103	140	101	137	128	97	153	102	78	83	100	89	145	111	109	113
Postcentral R	469	543	526	505	506	448	487	430	498	422	454	571	464	458	505	440	510	542	453	535	571	401	384	436
Posterior cingulate R	131	158	196	145	161	195	187	174	204	182	157	226	155	195	149	192	182	173	143	209	204	149	137	169
Precentral R	647	757	795	663	692	749	947	778	791	661	765	812	930	892	813	683	681	721	605	829	736	635	642	841
Precuneus R	520	724	749	582	562	631	755	553	752	716	582	671	602	732	716	765	560	757	550	828	613	600	513	770
Rostral anterior cingulate R	81	142	115	86	98	115	171	124	131	114	125	145	142	115	126	107	75	99	72	182	150	122	146	72
Rostral middle frontal R	757	1056	1079	1017	1035	1099	1202	918	1108	1375	878	1037	1013	1034	1177	1095	1021	1028	849	1400	1318	1172	1012	944
Superior frontal R	1162	1402	1351	1111	1380	1452	1543	1246	1570	1467	1376	1607	1345	1392	1266	1426	1235	1301	1151	1667	1678	1195	1170	1319
Superior parietal R	710	900	908	794	908	762	894	679	888	1017	811	838	794	946	777	890	662	805	645	811	860	772	691	883
Superior temporal R	607	742	693	667	658	862	751	754	722	799	727	814	697	774	720	773	716	808	630	871	799	770	648	808
Supramarginal R	566	812	819	658	645	708	769	524	787	723	634	835	703	762	657	883	705	724	552	874	740	787	518	669
Frontal pole R	56	52	60	63	54	74	67	49	56	125	56	68	55	57	65	62	61	66	55	84	82	87	75	55
Temporalpole R	103	173	118	138	109	99	163	134	194	148	131	125	134	153	165	168	163	119	157	157	188	148	139	154
Transverse temporal R	36	50	52	43	43	65	56	45	36	48	42	67	51	63	54	48	58	56	29	50	67	64	35	56
Insula R	341	436	413	352	406	527	450	336	468	451	383	478	453	449	399	463	390	468	363	491	517	413	427	426
Thalamus R	415	521	585	496	461	534	527	496	487	513	526	562	531	560	539	494	482	565	445	626	563	460	465	504
Thalamus L	189	261	250	183	229	228	254	229	231	279	277	218	238	246	273	249	244	257	203	284	241	231	235	312

L, left; R, right. Values are reflecting the subject-specific voxel numbers of each brain regions.

Supplementary Table 2. Volumes of rich-club regions for healthy controls (n=24) and at-risk mental state (ARMS) subjects (n=24).

	Healthy controls	**At risk mental state**	**Statistics**
Left Putamen	5237 ± 549	5380 ± 626	F=0.314, p=0.578
Left Pallidum	1499 ± 197	1542 ± 209	F=0.330, p=0.569
Left Accumbens	437 ± 91	430 ± 112	F=0.247, p=0.622
Left Caudate	3508 ± 510	3803 ± 464	F=3.182, p=0.081
Left Amygdala	1483 ± 154	1503 ± 199	F=0.039, p=0.844
Right Putamen	5017 ± 450	5261 ± 583	F=1.617, p=0.210
Right Pallidum	1337 ± 227	1439 ± 185	F=0.947, p=0.336
Right Accumbens	507 ± 92	503 ± 82	F=0.224, p=0.638

Values indicate mean volumes (in mm^3) ± standard deviation. Between-group statistics is controlled for total brain volume and gender.

Supplementary Figure 1. Overview of analytical workflow.

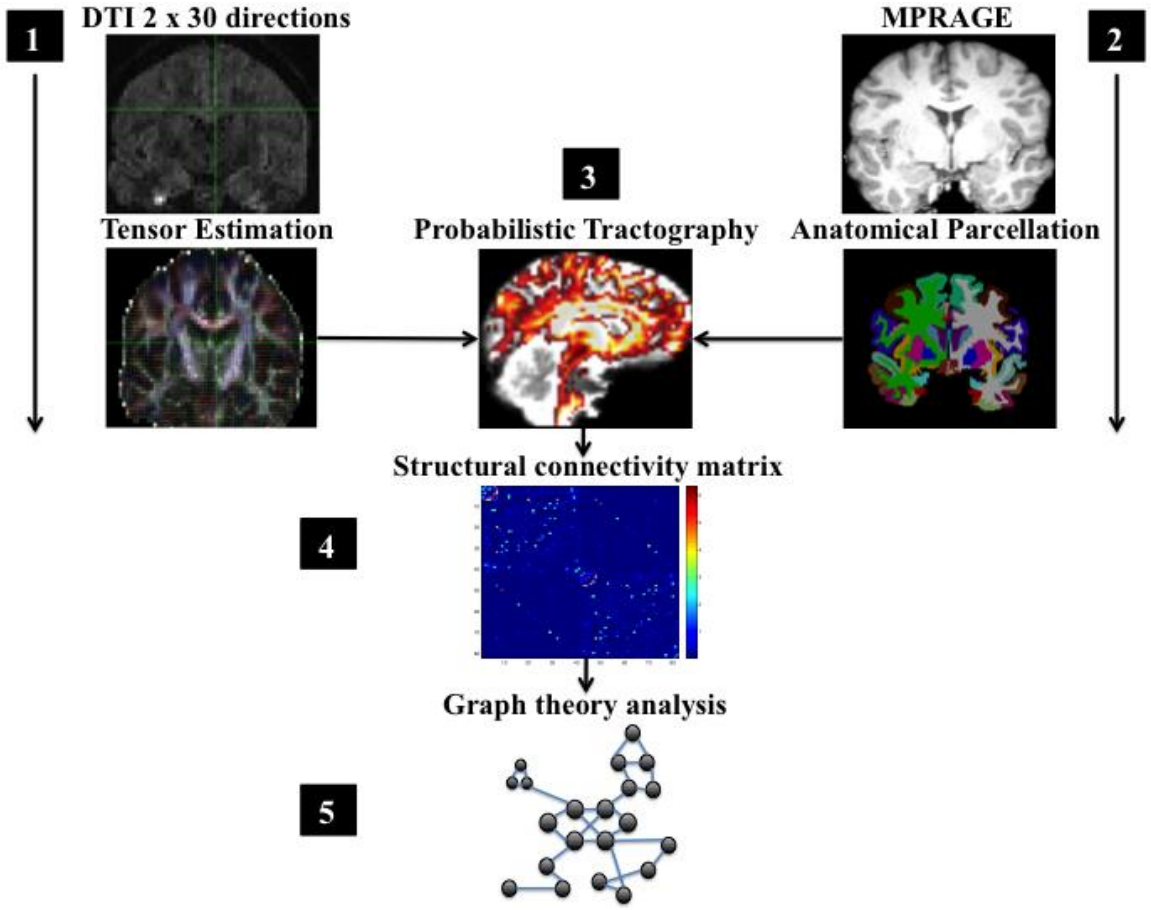

This figures summarizes the different methodological steps in the reconstruction of the individual structural network. **1.** First, DTI were acquired and preprocessed. **2.** In parallel, a high-resolution T1-weighted magnetization prepared rapid acquisition gradient echo (MPRAGE) images were used to segment 7 subcortical and 34 cortical brain regions per hemisphere. **3.** Probabilistic tractography was then conducted to estimate the probability of how many streamlines were connecting the 82 segmented brain regions. **4.** Connections were assembled into a subject-specific normalized weigthed connectivity matric. **5.** Different graph metrics were computed from these connectivity matrices.

Funding

This work was supported by the Swiss National Science Foundation (No. P2ZHP3_155184 to Dr. Schmidt).

Acknowledgments

The authors have declared that there are no conflicts of interest in relation to the subject of this study.

References

1. van den Heuvel MP, Fornito A. Brain networks in schizophrenia. *Neuropsychol Rev* 2014;24:32-48.

2. Fornito A, Zalesky A, Pantelis C, Bullmore ET. Schizophrenia, neuroimaging and connectomics. *Neuroimage* 2012;62:2296-2314.

3. Rubinov M, Bullmore E. Schizophrenia and abnormal brain network hubs. *Dialogues Clin Neurosci* 2013;15:339-349.

4. Bullmore E, Sporns O. Complex brain networks: graph theoretical analysis of structural and functional systems. *Nat Rev Neurosci* 2009;10:186-198.

5. Fornito A, Zalesky A, Breakspear M. The connectomics of brain disorders. *Nat Rev Neurosci* 2015;16:159-172.

6. Rubinov M, Bullmore E. Fledgling pathoconnectomics of psychiatric disorders. *Trends Cogn Sci* 2013;17:641-647.

7. Crossley NA, Mechelli A, Scott J, et al. The hubs of the human connectome are generally implicated in the anatomy of brain disorders. *Brain* 2014;137:2382-2395.

8. van den Heuvel MP, Mandl RC, Stam CJ, Kahn RS, Hulshoff Pol HE. Aberrant frontal and temporal complex network structure in schizophrenia: a graph theoretical analysis. *J Neurosci* 2010;30:15915-15926.

9. van den Heuvel MP, Sporns O, Collin G, et al. Abnormal rich club organization and functional brain dynamics in schizophrenia. *JAMA Psychiatry* 2013;70:783-792.

10. Wang Q, Su TP, Zhou Y, et al. Anatomical insights into disrupted small-world networks in schizophrenia. *Neuroimage* 2012;59:1085-1093.

11. Skudlarski P, Jagannathan K, Anderson K, et al. Brain connectivity is not only lower but different in schizophrenia: a combined anatomical and functional approach. *Biol Psychiatry* 2010;68:61-69.

12. Zalesky A, Fornito A, Seal ML, et al, Pantelis C. Disrupted axonal fiber connectivity in schizophrenia. *Biol Psychiatry* 2011;69:80-89.

13. Sun Y, Chen Y, Lee R, Bezerianos A, Collinson SL, Sim K. Disruption of brain anatomical networks in schizophrenia: A longitudinal, diffusion tensor imaging based study. *Schizophr Res* 2016;171:149-157.

14. Drakesmith M, Caeyenberghs K, Dutt A, et al. Schizophrenia-like topological changes in the structural connectome of individuals with subclinical psychotic experiences. *Hum Brain Mapp* 2015;36:2629-2643.

15. Ottet MC, Schaer M, Debbané M, Cammoun L, Thiran JP, Eliez S. Graph theory reveals dysconnected hubs in 22q11DS and altered nodal efficiency in patients with hallucinations. *Front Hum Neurosci* 2013;7:402.

16. Vása F, Griffa A, Scariati E, et al. An affected core drives network integration deficits of structural connectome in 22q11.2 deletion syndrome. *Neuroimage Clin* 2016;10:239-249.

17. Li Y, Liu B, Hou B, et al. Less efficient information transfer in Cys-allele carriers of DISC1: a brain network study based on diffusion MRI. *Cereb Cortex* 2013;23:1715-1723.

18. Shi F, Yap PT, Gao W, Lin W, Gilmore JH, Shen D. Altered structural connectivity in neonates at genetic risk for schizophrenia: a combined study using morphological and white matter networks. *Neuroimage* 2012;62:1622-1633.

19. van den Heuvel MP, Sporns O. Network hubs in the human brain. *Trends Cogn Sci* 2013;17:683-696.

20. van den Heuvel MP, Sporns O. Rich-club organization of the human connectome. *J Neurosci* 2011;31:15775-15786.
21. van den Heuvel MP, Sporns O. An anatomical substrate for integration among functional networks in human cortex. *J Neurosci* 2013;33:14489-14500.
22. Crossley NA, Mechelli A, Ginestet C, Rubinov M, Bullmore ET, McGuire P. Altered Hub Functioning and Compensatory Activations in the Connectome: A Meta-Analysis of Functional Neuroimaging Studies in Schizophrenia. *Schizophr Bull* 2016;42:434-442.
23. Collin G, Kahn RS, de Reus MA, Cahn W, van den Heuvel MP. Impaired Rich Club Connectivity in Unaffected Siblings of Schizophrenia Patients. *Schizophr Bull* 2014;40:438-448.
24. Fusar-Poli P, Borgwardt S, Bechdolf A, et al. The psychosis high-risk state: a comprehensive state-of-the-art review. *JAMA Psychiatry* 2013;70:107-120.
25. Johnstone EC, Lawrie SM, Cosway R. What does the Edinburgh high-risk study tell us about schizophrenia? *Am J Med Genet* 2002;114:906-912.
26. Smieskova R, Marmy J, Schmidt A, et al. Do subjects at clinical high risk for psychosis differ from those with a genetic high risk?--A systematic review of structural and functional brain abnormalities. *Curr Med Chem* 2013;20:467-481.
27. Fusar-Poli P, Bechdolf A, Taylor MJ, et al. At risk for schizophrenic or affective psychoses? A meta-analysis of DSM/ICD diagnostic outcomes in individuals at high clinical risk. *Schizophr Bull* 2013;39:923-932.
28. Fusar-Poli P, Bonoldi I, Yung AR, et al. Predicting psychosis: meta-analysis of transition outcomes in individuals at high clinical risk. *Arch Gen Psychiatry* 2012;69:220-229.
29. Riecher-Rössler A, Aston J, Ventura J, et al. [The Basel Screening Instrument for Psychosis (BSIP): development, structure, reliability and validity]. *Fortschr Neurol Psychiatr* Apr 2008;76:207-216.
30. Lukoff D, Liberman RP, Nuechterlein KH. Symptom monitoring in the rehabilitation of schizophrenic patients. *Schizophr Bull* 1986;12:578-602.
31. Andreasen NC. The Scale for the Assessment of Negative Symptoms (SANS): conceptual and theoretical foundations. *Br J Psychiatry Suppl* 1989:7:49-58.
32. Lehrl S, Triebig G, Fischer B. Multiple choice vocabulary test MWT as a valid and short test to estimate premorbid intelligence. *Acta Neurol Scand* 1995;91:335-345.
33. Yung AR, Phillips LJ, McGorry PD, et al. Prediction of psychosis. A step towards indicated prevention of schizophrenia. *Br J Psychiatry Suppl* 1998;172:14-20.
34. Fischl B. FreeSurfer. *Neuroimage* 2012;62:774-781.
35. Behrens TE, Woolrich MW, Jenkinson M, et al. Characterization and propagation of uncertainty in diffusion-weighted MR imaging. *Magn Reson Med* 2003;50:1077-1088.
36. Behrens TE, Berg HJ, Jbabdi S, Rushworth MF, Woolrich MW. Probabilistic diffusion tractography with multiple fibre orientations: What can we gain? *Neuroimage* 2007;34:144-155.
37. Cao Q, Shu N, An L, et al. Probabilistic diffusion tractography and graph theory analysis reveal abnormal white matter structural connectivity networks in drug-naive boys with attention deficit/hyperactivity disorder. *J Neurosci* 2013;33:10676-10687.
38. Gong G, Rosa-Neto P, Carbonell F, Chen ZJ, He Y, Evans AC. Age- and gender-related differences in the cortical anatomical network. *J Neurosci* 2009;29:15684-15693.

39. Colizza C, Flammini A, Serrano M, Vespignani A. Detecting rich-club ordering in complex networks. *Nat Phys* 2006;2:110-115.
40. Opsahl T, Colizza V, Panzarasa P, Ramasco JJ. Prominence and control: the weighted rich-club effect. *Phys Rev Lett* 2008;101:168702.
41. Rubinov M, Sporns O. Complex network measures of brain connectivity: uses and interpretations. *Neuroimage* 2010;52:1059-1069.
42. Newman ME. Modularity and community structure in networks. *Proc Natl Acad Sci U S A* 2006;103:8577-8582.
43. Schmidt A, Diwadkar VA, Smieskova R, et al. Approaching a network connectivity-driven classification of the psychosis continuum: a selective review and suggestions for future research. *Front Hum Neurosci* 2014;8:1047.
44. McGuire P, Sato JR, Mechelli A, Jackowski A, Bressan RA, Zugman A. Can neuroimaging be used to predict the onset of psychosis? *Lancet Psychiatry* 2015;2:1117-1122.
45. Schmidt A, Smieskova R, Aston J, et al. Brain connectivity abnormalities predating the onset of psychosis: correlation with the effect of medication. *JAMA Psychiatry* 2013;70:903-912.
46. Schmidt A, Palaniyappan L, Smieskova R, et al. Dysfunctional insular connectivity during reward prediction in patients with first-episode psychosis. *J Psychiatry Neurosci* 2016;41:150234.
47. Fusar-Poli P, Papanastasiou E, Stahl D, et al. Treatments of Negative Symptoms in Schizophrenia: Meta-Analysis of 168 Randomized Placebo-Controlled Trials. *Schizophr Bull* 2015;41:892-899.
48. Fusar-Poli P, Radua J, McGuire P, Borgwardt S. Neuroanatomical Maps of Psychosis Onset: Voxel-wise Meta-Analysis of Antipsychotic-Naive VBM Studies. *Schizophr Bull* 2012;38:1297-1307.
49. Mechelli A, Riecher-Rössler A, Meisenzahl EM, et al. Neuroanatomical abnormalities that predate the onset of psychosis: a multicenter study. *Arch Gen Psychiatry* 2011;68:489-495.
50. Haber SN, Fudge JL. The interface between dopamine neurons and the amygdala: implications for schizophrenia. *Schizophr Bull* 1997;23:471-482.
51. Grace AA. Phasic versus tonic dopamine release and the modulation of dopamine system responsivity: a hypothesis for the etiology of schizophrenia. *Neuroscience* 1991;41:1-24.
52. Egerton A, Chaddock CA, Winton-Brown TT, et al. Presynaptic striatal dopamine dysfunction in people at ultra-high risk for psychosis: findings in a second cohort. *Biol Psychiatry* 2013;74:106-112.
53. Howes OD, Bose SK, Turkheimer F, et al. Dopamine synthesis capacity before onset of psychosis: a prospective [18F]-DOPA PET imaging study. *Am J Psychiatry* 2011;168:1311-1317.
54. Fusar-Poli P, Meyer-Lindenberg A. Striatal Presynaptic Dopamine in Schizophrenia, Part II: Meta-Analysis of [18F/11C]-DOPA PET Studies. *Schizophr Bull* Jan 2013;39:33-42.
55. Winton-Brown TT, Fusar-Poli P, Ungless MA, Howes OD. Dopaminergic basis of salience dysregulation in psychosis. *Trends Neurosci* 2014;37:85-94.
56. Heinz A, Schlagenhauf F. Dopaminergic dysfunction in schizophrenia: salience attribution revisited. *Schizophr Bull* 2010;36:472-485.
57. Radua J, Schmidt A, Borgwardt S, et al. Ventral Striatal Activation During Reward Processing in Psychosis: A Neurofunctional Meta-Analysis. *JAMA Psychiatry* 2015;72:1243-1251.

58. Griffa A, Baumann PS, Ferrari C, et al. Characterizing the connectome in schizophrenia with diffusion spectrum imaging. *Hum Brain Mapp* 2015;36:354-366.
59. McColgan P, Seunarine KK, Razi A, et al. Selective vulnerability of Rich Club brain regions is an organizational principle of structural connectivity loss in Huntington's disease. *Brain* 2015;138:3327-3344.
60. Jones DK, Knösche TR, Turner R. White matter integrity, fiber count, and other fallacies: the do's and don'ts of diffusion MRI. *Neuroimage* 2013;73:239-254.
61. Collin G, de Nijs J, Hulshoff Pol HE, Cahn W, van den Heuvel MP. Connectome organization is related to longitudinal changes in general functioning, symptoms and IQ in chronic schizophrenia. *Schizophr Res* Apr 2016;173:166-173.
62. Drakesmith M, Caeyenberghs K, Dutt A, Lewis G, David AS, Jones DK. Overcoming the effects of false positives and threshold bias in graph theoretical analyses of neuroimaging data. *Neuroimage* 2015;118:313-333.

Tables

Table 1. Clinical and demographic characteristics of the study sample.

	HC (n=24)	**ARMS group (n=24)**	**Group statistics**
Age (years, mean ± SD)	27.75 ± 4.59	25.42 ± 6.74	$t_{46} = 1.400$; $p = 0.170$
Gender (female/male)	14/10	6/18	$\chi^2 = 5.486$; $p = 0.019$
Handedness (right)	22	22	$\chi^2 = 0.000$; $p = 1$
Education (years, mean ± SD)	15.38 ± 2.92	15.04 ± 3.39	$t_{46} = 0.365$; $p = 0.717$
Premorbid IQ (MWT-B, mean ± SD)	120 ± 11.06	115 ± 14.27	$t_{46} = 1.187$; $p = 0.242$
Cigarettes smoked per day (mean ± SD)	4.08 ± 7.01	6.00 ± 8.20	$t_{46} = -0.871$; $p = 0.389$
Alcohol consumption (no/moderate/uncontrolled)	1/21/2	4/18/2	$\chi^2 = 2.031$; $p = 0.362$
Number of subjects consuming cannabis	4	5	$\chi^2 = 0.000$; $p = 1$
GAF total score (mean ± SD)	88.63 ± 4.39	68.75 ± 11.8	$t_{46} = 7.733$; $p < 0.001$
BPRS total score (mean ± SD)	24.59 ± 1.14	38.71 8.24	$t_{46} = -7.963$; $p < 0.001$
SANS total score (mean ± SD)	0	24.33 ± 14.20	$t_{46} = -7.126$; $p < 0.001$

ARMS, at-risk mental state; BPRS, Brief Psychiatric Rating Scale; GAF, Global Assessment of Functioning; HC, healthy controls; MWT-B, Mehrfachwahl-Wortschatz-Test Form B; (Multiple Choice Vocabulary Test); SANS, Scale for the Assessment of Negative Symptoms; SD, standard deviation.

Figure Legends

Figure 1. Normalized rich-club coefficient (Φ^{w}_{norm}) at different rich-club levels expressed as the percentile of node strength for healthy controls (n=24) and at-risk mental state (ARMS) subjects. (*) significantly reduced Φ^{w}_{norm} in ARMS subjects compared to healthy controls.

Figure 2. A) Structural network organization. Rich-club regions, including the bilateral putamen, pallidum, accumbens and the left caudate and amygdala and their connections among each other are depicted in yellow, while feeder connections are depicted in green and local connections in blue. Dotplots represent strength of **B)** rich-club **C)** feeder and **D)** local connections in at risk mental state (ARMS) subjects compared and healthy controls. (**) significant group difference at p=0.0207, (*) statistical trend for group difference at p=0.0549.

Figure 3. (A) Modularity values in healthy controls and in at-risk mental state (ARMS) subjects. **(B)** Negative relation between the area under the rich-club curve and modularity across all participants (r=-0.388, p=0.007). **(C)** Efficiency values of the right accumbens in healthy controls and in at-risk mental state (ARMS) subjects. **(D)** Clustering values of the left accumbens in healthy controls and in at-risk mental state (ARMS) subjects. **(*)** significant group differences.

Figure 4. A) In at-risk mental state (ARMS) subjects, negative psychotic symptoms were inversely related to the area under the rich-club curve (r=-0.506, p=0.012). Across all participants, global functioning were **B)** positively related to the area under the rich-club curve (r=0.440, p=0.002) and **C)** negatively related to modularity (r=-0.305, p=0.035).